THE JOURNAL OF BIOLOGICAL CHEMISTRY VOL. 291, NO. 9, pp. 4671–4683, February 26, 2016
© 2016 by The American Society for Biochemistry and Molecular Biology, Inc. Published in the U.S.A.

Molecular Basis of Enhanced Activity in Factor VIIa-Trypsin Variants Conveys Insights into Tissue Factor-mediated Allosteric Regulation of Factor VIIa Activity*[S]

Received for publication, October 16, 2015, and in revised form, December 15, 2015 Published, JBC Papers in Press, December 22, 2015, DOI 10.1074/jbc.M115.698613

Anders B. Sorensen[‡§1], Jesper J. Madsen[‡¶1,2], L. Anders Svensson[‡], Anette A. Pedersen[‡], Henrik Østergaard[‡], Michael T. Overgaard[§], Ole H. Olsen[‡], and Prafull S. Gandhi[‡3]

From [‡]Global Research, Novo Nordisk A/S, 2760 Måløv, Denmark, [§]Department of Chemistry and Bioscience, Aalborg University, 9220 Aalborg, Denmark, and [¶]Department of Chemistry, Technical University of Denmark, 2800 Kongens Lyngby, Denmark

The complex of coagulation factor VIIa (FVIIa), a trypsin-like serine protease, and membrane-bound tissue factor (TF) initiates blood coagulation upon vascular injury. Binding of TF to FVIIa promotes allosteric conformational changes in the FVIIa protease domain and improves its catalytic properties. Extensive studies have revealed two putative pathways for this allosteric communication. Here we provide further details of this allosteric communication by investigating FVIIa loop swap variants containing the 170 loop of trypsin that display TF-independent enhanced activity. Using x-ray crystallography, we show that the introduced 170 loop from trypsin directly interacts with the FVIIa active site, stabilizing segment 215–217 and activation loop 3, leading to enhanced activity. Molecular dynamics simulations and novel fluorescence quenching studies support that segment 215–217 conformation is pivotal to the enhanced activity of the FVIIa variants. We speculate that the allosteric regulation of FVIIa activity by TF binding follows a similar path in conjunction with protease domain N terminus insertion, suggesting a more complete molecular basis of TF-mediated allosteric enhancement of FVIIa activity.

Allosteric mechanisms play a vital role in the timely initiation and progression of the blood coagulation cascade. At the site of injury, membrane-bound tissue factor (TF)[4] interacts with zymogen coagulation factor VII (FVII) and its active form (FVIIa). The FVIIa·TF complex initiates the coagulation cascade by activating FIX and FX, leading to thrombin generation and eventually wound healing (1). Conversion of FVII to FVIIa involves proteolytic cleavage at the Arg^{15}-Ile^{16} peptide bond,[5] producing a disulfide-linked two-chain molecule with a light chain consisting of a phospholipid-interactive γ-carboxyglutamic acid domain, two epidermal growth factor (EGF)-like domains, and a heavy chain trypsin-like protease domain (2) (Fig. 1*A*). In trypsin, the N terminus formed upon activation spontaneously enters the activation pocket to form a salt bridge with residue Asp^{194}. This key interaction leads to optimal alignment and architecture of the oxyanion hole and primary specificity pocket (S1), resulting in a mature active site for substrate binding and catalysis (3). In FVIIa, the newly formed N terminus fails to completely insert into the activation pocket (4), leading to a non-optimal configuration of the catalytic machinery, rendering FVIIa "zymogen-like" with inferior catalytic efficiency. TF binding allosterically corrects these defects in the catalytic domain by stabilizing the 170 loop (amino acids 170–178) in conjunction with activation loops 1–3 (AL1–3) and promotes N terminus insertion (Fig. 1*B*) (5, 6). This transforms FVIIa into its catalytically competent form and increases amidolytic activity by 40-fold (7). Furthermore, TF ensures optimal orientation and positioning of the FVIIa catalytic domain above the membrane surface and generates exosites for incoming macromolecular substrates, thereby enhancing the proteolytic activity by ~10^5-fold (8, 9).

Previous studies have provided details of TF-binding regions in the FVIIa light chain and on structural changes in the protease domain upon cofactor binding. However, the full extent of TF-mediated structural changes has yet to be fully elucidated, and key components of the allosteric pathways remain elusive (10). To further understand the molecular basis of TF-mediated allosteric regulation of FVIIa activity, we considered FVIIa variants displaying superior catalytic efficiency in the absence of TF, variants modified in the vicinity of either the 170 loop (11) or the activation pocket (7), or a variant with the 170 loop replaced by that of trypsin (FVIIa-Y_T) (12). Interestingly, FVIIa-Y_T displays a similar extent of N terminus insertion as FVIIa wild type (WT) in the absence of TF; however, FVIIa-Y_T displays improved catalytic efficiency. Recent studies with thrombin, another trypsin-like serine protease, reveal a highly plastic protease fold for the apo form of thrombin that undergoes structural transitions upon cofactor binding (13–19). In particular, segment 215–217 was shown to be vital for substrate

* A. B. S., L. A. S., A. A. P., H. Ø., O. H. O., and P. S. G. are employees of Novo Nordisk A/S.

The atomic coordinates and structure factors (codes 4z6a, 4zma, and 4ylq) have been deposited in the Protein Data Bank (http://wwpdb.org/).

[S] This article contains supplemental Movies S1–S5.

[1] Supported by grants from the Danish Agency for Science, Technology and Innovation and the Novo Nordisk Research and Development Science Talent Attraction and Recruitment (STAR) program.

[2] Present address: Dept. of Chemistry, The University of Chicago, Chicago, IL 60637.

[3] To whom correspondence should be addressed: Protein Interaction, Novo Nordisk A/S, Novo Nordisk Park, G8.2.61, DK-2760 Måløv, Denmark. Tel.: 45-3079-9829; E-mail: pgan@novonordisk.com.

[4] The abbreviations used are: TF, tissue factor; sTF, soluble tissue factor 1–219; FVIIa, activated coagulation factor VIIa; FVII, zymogen coagulation factor VII; AL1–3, activation loops 1–3; MD, molecular dynamics; SASA, solvent-accessible surface area; FFR, H-D-Phe-Phe-Arg chloromethyl ketone TFA salt; S-2288, D-Ile-Pro-Arg-*p*-nitroanilide; pABA, *p*-aminobenzamidine; K_{sv}, Stern-Volmer quenching constant.

[5] Chymotrypsin numbering used throughout the article.

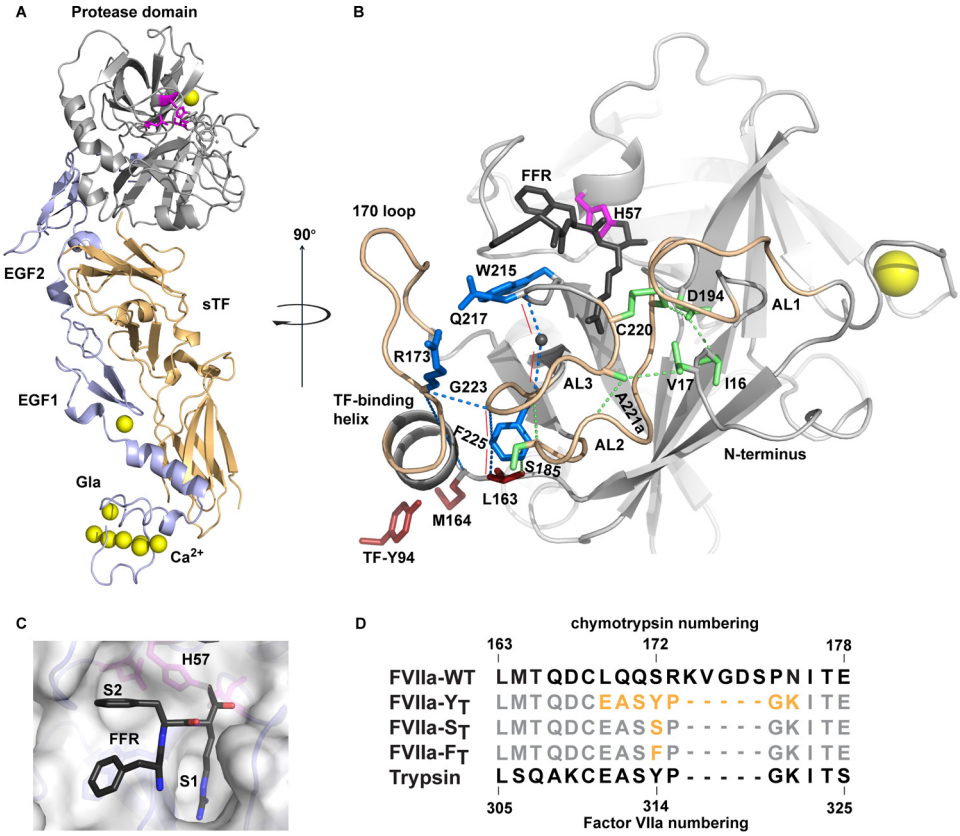

FIGURE 1. **Overview of the FVIIa-WT·sTF complex and variant nomenclature.** *A*, full view of the FVIIa-WT·sTF (Protein Data Bank code 1dan) complex with the FVIIa protease domain in *gray*, light chain in *blue*, sTF in *orange*, Ca^{2+} ions in *yellow*, and the active site triad in *magenta*. The phospholipid-interactive γ-carboxyglutamic acid (*Gla*) domain and EGF-like domain are shown. *B*, FVIIa-WT protease domain with the 170 loop (residues 170–178), AL1 (residues 142–152), AL2 (residues 184–193), and AL3 (residues 220–225) in *sand*. Residues suggested to be involved in TF-induced enhancement in FVIIa activity through allosteric pathways I (*blue*) and II (*green*) are shown with *connecting dotted lines*. Common residues for both pathways from Tyr^{94} in TF are shown in *red*. FFR is shown in *black*. New sections of the pathways suggested here are marked with *red fully drawn lines*. *C*, FFR inhibitor (*black*) shown in the active site of FVIIa with substrate subsites 1 and 2 marked. *D*, sequence alignment of FVIIa-WT, trypsin, and the FVIIa variants with mutations highlighted (*orange*).

access and cofactor-mediated allosteric regulation, which may also be the case in TF-mediated allosteric regulation of FVIIa activity (20, 21).

We hypothesized that the improved catalytic efficiency of FVIIa-Y_T is due to stabilization of the 215–217 segment with Tyr^{172} playing an important role. To test our hypothesis, we investigated the FVIIa-Y_T variant and two variants of FVIIa-Y_T where this tyrosine is either replaced by serine (FVIIa-S_T) or phenylalanine (FVIIa-F_T) (Fig. 1*D*). Data presented here confirm that Tyr^{172} stabilizes the 215–217 segment and AL3 in the absence of TF, maturing the primary specificity pocket and enhancing catalytic efficiency independently of complete protease domain N terminus insertion. Molecular dynamics (MD) simulations supported the experimental results and suggested the direct involvement of Trp^{215} in TF-mediated allosteric changes in the protease domain, further corroborated by fluorescence quenching studies and solvent-accessible surface area (SASA) calculations. Based on these observations, we hypothesize that stabilization of segment 215–217 in the open conformation is a key step in TF-mediated allosteric regulation of FVIIa.

Experimental Procedures

Materials—H-D-Phe-Phe-Arg chloromethyl ketone TFA salt (FFR) was from Bachem (Basel, Switzerland). D-Ile-Pro-Arg *p*-nitroanilide (S-2288) was from Chromogenix (Mölndal, Sweden). All other chemicals were from Sigma-Aldrich and of analytical grade or the highest quality commercially available. Recombinant wild-type human FVIIa was prepared as described previously (11). Recombinant human soluble tissue factor 1–219 (sTF) was prepared as described (22) with the modification of using the reductase-deficient *Escherichia coli* strain BL21 Origami (Novagen, Germany). Factor Xa was purchased from Molecular Innovations.

Factor VII Mutagenesis and Protein Expression—Human wild-type FVII cDNA was cloned into a QMCF vector (Icosagen AS, Estonia), and all variants were generated using a PCR-based site-directed mutagenesis method with KOD Xtreme Hot Start DNA polymerase (Novagen) or a QuikChange Lightning XL (Agilent) kit according to the manufacturers' instructions. Introduction of the desired mutations was verified by DNA sequencing of the entire FVII cDNA region (MWG Biotech, Germany). QMCF Technology, a semistable episomal mammalian expression system obtained from Icosagen AS (Estonia), was used for expression of the FVII variants in a QMCF CHO cell line (CHO-EBNALT85), and cells were cultivated according to the manufacturer's instructions. During a period of 3–4 weeks, the transfected cell cultures were expanded to 2–10 liters, and the media were harvested by centrifugation and 0.22-μm filtration.

Protein Purification and Verification—For all FVII variants, expression medium was adjusted to pH 6.0, $CaCl_2$ was added to 5 mM, and benzamidine HCl was added to a final concentration of 10 mM. All purification steps were performed using an ÄKTA Explorer system (GE Healthcare) and consisted of an immunoaffinity purification step (γ-carboxyglutamic acid domain-specific) performed as described (23) except at pH 6.0 using a histidine buffer and eluting with 20 mM EDTA. This was followed by a concentration and purification step using a prepacked 6-ml ResourceQ™ (GE Healthcare) column at pH 6.0, eluting with a step gradient to 100 mM NaCl, 60 mM $CaCl_2$ in 10 mM histidine. Activation of FVII variants was performed by passing the protein solution through a custom packed Tricon column (GE Healthcare) with factor Xa coupled to Sepharose 4B FF CNBr (GE Healthcare). Protein identity was verified using intact electrospray ionization-TOF mass spectrometry, and purity was shown to be >95% by Novex 4–12% SDS-PAGE (Life Technologies). The amount of active protein was determined by active site titration using FFR and measuring residual S-2288 activity (24).

Functional Evaluation of FVIIa 170 Loop Variants—All functional assays were carried out in 50 mM Hepes, pH 7.4, 0.1 M NaCl, 5 mM $CaCl_2$, 0.01% Tween 20 (assay buffer) and monitored at 405 nm in a microplate reader (SpectraMax 340, Molecular Devices Corp., Sunnyvale, CA) using a Nunc F96-well plate (non-treated clear) with a 200-μl assay volume at 25 °C. sTF binding studies using S-2288 were performed essentially as described (12) using 0–3 μM sTF. Kinetic parameters of S-2288 hydrolysis were determined for the FVIIa variants with 0–12.5 mM S-2288, and the K_i for inhibition by pABA was determined in a competitive activity assay using 1 mM S-2288 as described (11). Carbamylation of the N-terminal Ile^{16} was investigated by incubating in 0.2 M KNCO (Sigma-Aldrich) and measuring residual activity at 1 mM S-2288 as described (11). All functional studies were performed in the absence or presence of 3 μM sTF. Data analysis and curve fitting were performed using GraphPad Prism 6.0.

FVIIa Variant Preparation, Crystallization, and Data Collection—Preparation of samples for x-ray crystallography was performed by inhibiting FVIIa-Y_T, -S_T, and -F_T with FFR and adding sTF in a 1:1 molar relationship. Protein integrity was verified using SDS-PAGE. Diffraction quality crystals were obtained using the hanging drop method at 22 °C with two different conditions: for FVIIa-Y_T and -F_T, 0.1 M sodium citrate buffer at pH 5.1, 16.6% PEG 3350 (Hampton Research), 12.5% 1-propanol, and for FVIIa-S_T, 0.1 M cacodylate buffer at pH 5.6, 12% PEG 8000 (Hampton Research). All diffraction data were collected at MaxLab IV beam-line I911-3 (25). Data were integrated and scaled using the XDS package (26). Molecular replacement was performed with the Phenix.Phaser software (27) and a FVIIa-WT·sTF-FFR complex as a search model. The subsequent refinement and model building were performed using iterative cycles of Phenix.Refine (28) in the Phenix program package (29), utilizing MolProbity (30) and TLS (31), followed by computer graphic model corrections by Coot software (32). The three generated structures were deposited in the Protein Data Bank as FVIIa-Y_T (Protein Data Bank code 4z6a), FVIIa-S_T (Protein Data Bank code 4zmA), and FVIIa-F_T (Protein Data Bank code 4ylq).

Acrylamide Tryptophan Quenching—Fluorescence intensity measurements were performed on a Cary Eclipse spectrofluorometer (Agilent Technologies) equipped with a four-cell magnetic stirrer sample holder and Peltier element using a set of four 10 × 10-mm QS quartz cuvettes (Hellma Analytics, Germany). 150 nM FVIIa variant in assay buffer kept at 15, 25, or 37 °C was titrated with 0–0.5 M acrylamide using a volume replacement approach by preparing two identical solutions for the titration where one was spiked with 5.63 M acrylamide (Bio-Rad). Data were collected with excitation at 295 nm (5-nm slit width) and emission at 330 nm (20-nm slit width); the integration time was 0.5 s. The collected data were baseline-corrected, and inner filtering effects were addressed by a correction method for a right-angled fluorescence setup (33) with the correction factor being $F_{corr} = F_{obs} \times 10^{0.125 \times [acrylamide]}$ using a ϵ_{295} of 0.25 M^{-1} cm^{-1} for acrylamide and a path length of fluorescence measurement of 0.5 cm. Stern-Volmer plots were generated, and the data were analyzed using a dynamic collision quenching model (34) in GraphPad Prism 6.0.

$$\frac{F_0}{F} = 1 + K_{sv}[Q] \qquad \text{(Eq. 1)}$$

The observed correlation between the determined Stern-Volmer quenching constant (K_{sv}) values and the calculated SASA values was evaluated using a Pearson correlation approach in GraphPad Prism 6.0 to determine whether it could be explained by random sampling ($\alpha = 0.01$).

Molecular Dynamics Simulations of FVIIa Variants—For MD simulations, the FVIIa 170 loop variants were constructed using the x-ray crystallographic structure of FVIIa-Y_T as a template. For the S_T and F_T variants, Tyr^{172} was mutated to Ser and Phe, respectively, while preserving the side chain rotamer of the template. FVIIa-WT was based on a representative structure of benzamidine-inhibited FVIIa (Protein Data Bank code 1kli (35)). The complex of sTF 1–213 and FVIIa was constructed starting from Protein Data Bank code 1dan as described and graciously provided by Ohkubo *et al.* (8). In all structures, the co-crystallized inhibitor was removed. 100-ns conventional MD simulations of the FVIIa-WT·sTF complex, FVIIa-WT, and the three FVIIa variants with the trypsin 170 loops were performed using the NAMD 2.7 software package (36) with the CHARMM27 force field (37) and the TIP3P water model (38). An integration time step of 1.0 fs was used for the velocity Verlet algorithm. Simulations were carried out at constant pressure (P = 1 atm) and constant temperature (T = 310 K) controlled by the Langevin thermostat (damping coefficient, 5/ps) and the Nosé-Hoover Langevin piston barostat (39, 40), respectively. Throughout, anisotropic pressure coupling was applied for the barostat using a piston damping coefficient of 5/ps, a piston period of 100 fs, and piston decay of 50 fs. Long range electrostatic forces were calculated using the particle mesh Ewald method (41) using a grid spacing of ~1 Å and a fourth order spline for interpolation. Electrostatic forces were updated every 4th fs. van der Waals interactions were cut off at 12 Å in combination with a switching function beginning at 10

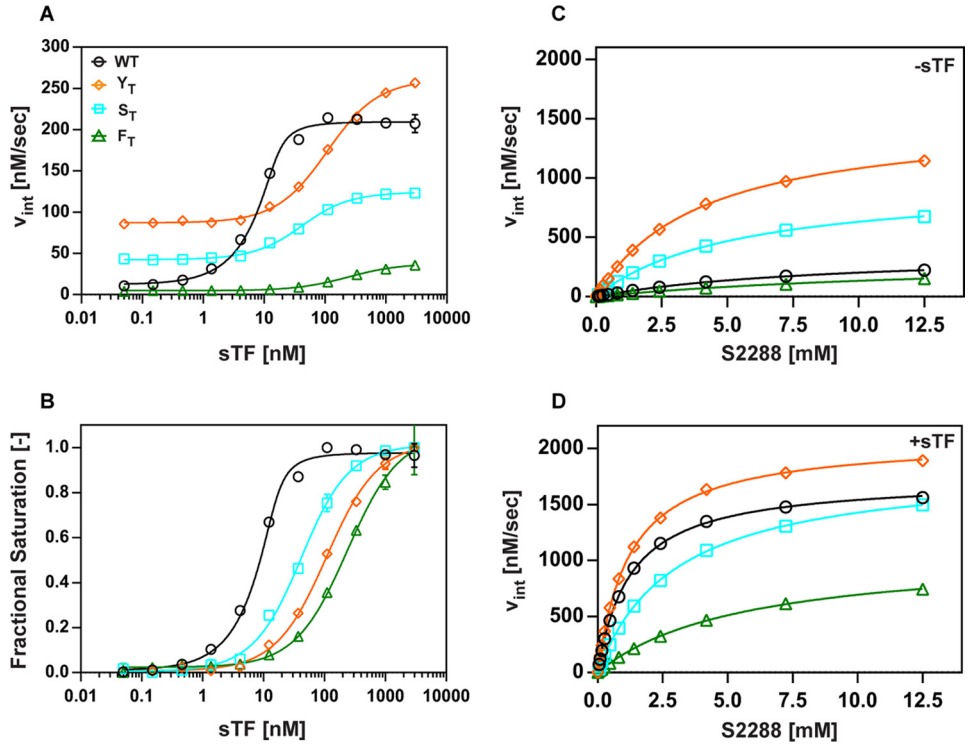

FIGURE 2. **Cofactor binding and amidolytic activity of FVIIa variants.** *A*, initial velocity (V_{int}) of 1 mM S-2288 hydrolysis by 15 nM FVIIa-WT (○) in *black*, FVIIa-Y_T (◇) in *orange*, FVIIa-S_T (□) in *cyan*, and FVIIa-F_T (△) in *green* as a function of sTF concentration (0–3 μM). Data are presented as the mean with *error bars* showing the highest and lowest data points ($n = 2$) and were fitted with a quadratic equilibrium equation. *B*, sTF fractional saturation of FVIIa variants using S-2288 activity. Data were normalized and fitted with a quadratic equilibrium equation. Data are presented as the mean with *error bars* showing the highest/lowest data points ($n = 2$). *C* and *D*, initial velocity values for hydrolysis of S-2288 without or with 3 μM sTF. Data were fitted with a Michaelis-Menten equation using non-linear regression. Data are presented as the mean with *error bars* showing the highest and lowest data points ($n = 2$) at 25 °C.

Å. Periodic boundary conditions was applied in *x*-, *y*-, and *z*-directions. The potential energy in all systems was initially minimized using 500 steps of the conjugated gradient method.

SASA—The SASA was calculated for all tryptophans in the simulated FVIIa variants during the entire time course at a probe radius of 1.4 Å using the standard implementation (*measure* command) in VMD (42). The same calculations were made for the crystal structures with FFR present. For graphical comparison of SASA values for Trp^{215} between variants, the data were smoothened using the Savistsky and Golay method in GraphPad Prism 6.0 with a window size of 10 and a second degree polynomial.

Results

The 170 Loop Is Linked to Cofactor Binding and Amidolytic Activity—Previous studies have shown that the conformation of the 170 loop is affected by the binding of TF to FVIIa (2, 6). In agreement, impairment of cofactor interaction was observed for the three FVIIa variants as assessed by the effect of sTF on FVIIa amidolytic activity (S-2288) (Fig. 2, *A–D*, and Table 1). FVIIa-Y_T displayed an 84-fold compromise in its ability to bind to sTF but could be fully stimulated by the addition of saturating sTF, reaching a higher final amidolytic activity than FVIIa-WT·sTF (Fig. 2, *A* and *D*). This indicates that the engineered 170 loop in FVIIa-Y_T selectively affects sTF binding but is still able to mediate allosteric communication to the FVIIa active site upon sTF binding. From the kinetics of S-2288 hydrolysis, we found that the increased FVIIa-Y_T activity at saturating sTF concentration was entirely due to an increased k_{cat} value with no change in the K_m value compared with the FVIIa-WT·sTF complex (Fig. 2*D* and Table 1). In addition, we reproduced the higher activity of FVIIa-Y_T without sTF with an increase in k_{cat}/K_m of 8.3-fold over FVIIa-WT (12). The importance of Tyr^{172} was evident as the removal of a single hydroxyl group (FVIIa-F_T) resulted in a markedly decreased potentiation of activity and a loss in sTF affinity (Fig. 2, *A* and *B*, and Table 1) with an accompanying reduction of the intrinsic activity to half that of FVIIa-WT (Fig. 2*C* and Table 1). The FVIIa-S_T variant showed a partial rescue of sTF affinity (Table 1), maintaining a 4-fold higher intrinsic activity compared with FVIIa-WT,

TABLE 1

Functional investigation of 170 loop variants

Dissociation constants ($K_{d,app}$, nM) for FVIIa-WT (1.2 ± 0.3), -Y_T (101.6 ± 4.1), -S_T (34.2 ± 2.0), and -F_T (231.1 ± 22.8) were determined by S-2288 activity measurements. S-2288 amidolytic kinetic constants, pABA inhibition values, and carbamylation half-life are shown as means with calculated S.E. in parentheses ($n = 2$) at 25 °C.

	S-2288 K_M	S-2288 k_{cat}	k_{cat}/K_M	pABA K_i	KNCO $t_{½}$
	mM	s^{-1}	s^{-1}/mM	*μM*	*min*
−sTF					
FVIIa-WT	8.9 (0.4)	7.7 (0.2)	0.9 (0.02)	1485.0 (87.7)	43.9 (1.0)
FVIIa-Y_T	4.0 (0.1)	30.4 (0.5)	7.5 (0.2)	97.6 (10.1)	40.8 (0.5)
FVIIa-S_T	5.3 (0.2)	19.3 (0.3)	3.6 (0.1)	190.4 (13.1)	43.8 (0.6)
FVIIa-F_T	15.4 (1.3)	6.8 (0.4)	0.4 (0.01)	490.3 (46.3)	32.4 (0.7)
+sTF					
FVIIa-WT	1.2 (0.03)	34.6 (0.2)	28.0 (0.4)	49.3 (1.8)	536.2 (39.6)
FVIIa-Y_T	1.2 (0.02)	41.7 (0.2)	34.4 (0.5)	24.7 (1.2)	56.7 (0.9)
FVIIa-S_T	3.0 (0.06)	37.1 (0.3)	12.4 (0.2)	41.7 (1.3)	159.0 (4.8)
FVIIa-F_T	5.6 (0.1)	21.6 (0.3)	3.9 (0.1)	69.5 (3.7)	37.1 (0.7)

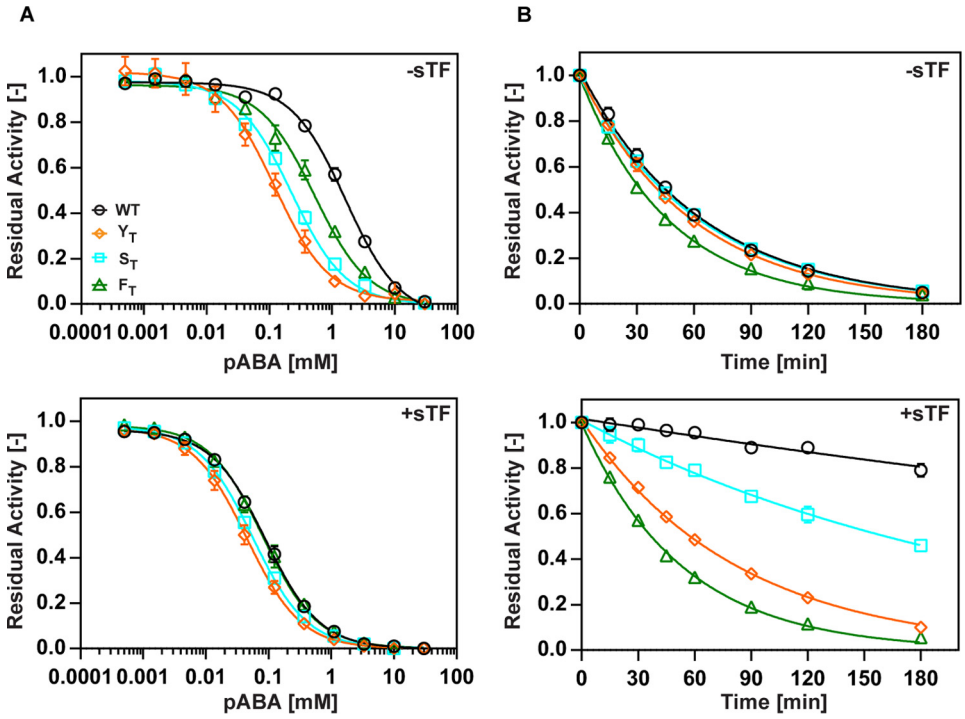

FIGURE 3. **Functional characterization of FVIIa variants.** *A*, titration of 10–100 nM FVIIa-WT (○) in *black*, FVIIa-Y_T (◇) in *orange*, FVIIa-S_T (□) in *cyan*, and FVIIa-F_T (△) in *green* with 0–30 mM pABA inhibitor normalized to residual activity in the presence of 1 mM S-2288. Data were fitted with a competitive inhibition equation. Data are presented as the mean with *error bars* showing the highest and lowest data points ($n = 2$). *Top panel*, without sTF; *bottom panel*, with 3 μM sTF. *B*, carbamylation assay with 0.2 M KNCO monitoring residual S-2288 activity as a function of time fitted with a single exponential decay function. Data are presented as the mean with *error bars* showing the highest and lowest data points ($n = 2$) at 25 °C.

whereas the activity level at saturating sTF concentration was significantly reduced (Fig. 2*A* and Table 1). Independent surface plasmon resonance analysis confirmed sTF affinity values for the three FVIIa variants obtained by the amidolytic activity strategy (data not shown).

Inhibitor Binding Reveals Changes in S1 Pocket Maturation—To further investigate the effect of the engineered 170 loops on the active site, we probed the S1 pocket by binding of pABA, a small molecule inhibitor known to occupy the S1 pocket and oxyanion hole (35). Consistent with an immature S1 pocket, FVIIa-WT was poorly inhibited by pABA in the absence of sTF (K_i 1485 μM; Fig. 3*A* and Table 1). The K_i values for FVIIa-Y_T and FVIIa-S_T were significantly decreased in agreement with their increased amidolytic activity and a more mature S1 pocket (Table 1). FVIIa-F_T exhibited an intermediate K_i value. Binding of sTF to FVIIa-WT is known to mature the active site (23) and resulted in a ~30-fold decreased K_i value (49.3 μM). At saturating sTF concentrations, FVIIa-WT, FVIIa-Y_T, FVIIa-S_T, and FVIIa-F_T all reached similar K_i values (Fig. 3*A* and Table 1) as anticipated for FVIIa-Y_T and FVIIa-S_T but not for FVIIa-F_T due to its much lower activity toward S-2288. This suggests that FVIIa-F_T has a mature S1 pocket in the presence of sTF but possibly impaired substrate binding in the S2-S3 pockets.

Mutagenesis of the 170 Loop Affects N Terminus Protection—A functional marker for FVIIa "zymogenicity" is the extent of N terminus insertion, which can be perturbed by TF binding or by mutagenesis in FVIIa (7, 12). The carbamylation assay (Fig. 3*B* and Table 1) correlates Ile^{16} (N terminus) solvent exposure to residual activity and has been successfully used to assess the extent of protease domain N terminus insertion (4). In the absence of sTF, FVIIa-WT, FVIIa-Y_T, and FVIIa-S_T showed similar levels of N terminus protection, whereas the protection level was slightly decreased in FVIIa-F_T (Fig. 3*B*). Addition of sTF had a pronounced effect on N terminus insertion with FVIIa-WT showing complete protection, whereas FVIIa-Y_T achieves very little protection, suggesting that the improved amidolytic activity observed for this variant is independent of complete N terminus insertion. Interestingly, the FVIIa-S_T N terminus is protected when compared with FVIIa-Y_T, correlating with the increased sTF affinity, whereas FVIIa-F_T showed the lowest level of protection gained from sTF addition in agreement with a poor catalytic activity and sTF affinity.

Tyr^{172} Directly Stabilizes Segment 215–217 and AL3—To investigate the conformation of the 170 loop from trypsin in FVIIa, we determined the x-ray crystal structure of the three variants with sTF and the irreversible active site inhibitor FFR (2). The three FVIIa variants crystallized in identical space groups with highly similar unit cell dimensions, allowing meaningful structural comparison. Data collection and refinement statistics are summarized in Table 2. Comparison of the protease domain of FVIIa-WT (Protein Data Bank code 1dan (2)) and the three variants revealed the same structural topology (Cα root mean square deviation of the protease domain (241 residues) of 0.27–0.39 Å) outside the immediate surroundings of the 170 loop and AL2–3 (residues 184–193 and 220–225) (Fig. 4, *A–D*). The FVIIa-Y_T map ($2F_o - F_c$) lacked electron density for the Ca^{2+}-dependent γ-carboxyglutamic acid domain presumably due to the presence of citrate in the crystallization condition and the cryoprotectant for this variant.

TABLE 2
Data collection and refinement statistics of x-ray crystallography

	FVIIa-Y_T	FVIIa-S_T	FVIIa-F_T
Protein Data Bank code	4z6a	4zma	4ylq
Data collection			
Wavelength (Å)	1.00	1.00	1.00
Space group	$P2_12_12_1$	$P2_12_12_1$	$P2_12_12_1$
Cell dimensions			
a, *b*, *c* (Å)	67.0, 81.7, 124.6	66.2, 80.9, 125.8	71.3, 80.0, 123.4
α, β, γ (°)	90, 90, 90	90, 90, 90	90, 90, 90
Molecules/asymmetric unit	1	1	1
Resolution range (Å)	29.1–2.25 (2.33–2.25)[a]	29.8–2.3 (2.4–2.3)	33.6–1.4 (1.45–1.40)
Total reflections	155,080	104,023	1,008,907
Unique reflections	32,039	29,510	138,937
Completeness (%)	97.0 (81.0)	96.1 (87.4)	1.00 (0.98)
R_{merge}	0.14 (1.4)	0.16 (1.9)	0.09 (2.1)
$I/\sigma I$	10.0 (0.97)	8.7 (0.78)	14.1 (0.83)
Refinement			
Resolution (Å)	29.1–2.25	29.8–2.3	33.6–1.4
R_{work}/R_{free}	0.19/0.24	0.24/0.29	0.14/0.17
Reflections[b] (working/test)	32,039/1,605	29,510/1,500	138,932/6,917
r.m.s.[c] deviations			
Bond lengths (Å)	0.003	0.002	0.024
Bond angles (°)	0.83	0.59	4.09
Wilson B-factor	36.9	33.4	15.3
Average atomic B-factors			
Protein	45.6	38.2	22.4
Ligands	59.9	54.8	46.0
Solvent	38.7	33.8	33.2
Ramachandran			
Favored (%)	97.2	94.6	97.5
Allowed (%)	2.8	5.4	2.5
Outliers (%)	0	0	0

[a] Highest resolution shell.
[b] Cutoff used in refinement was $F > 0\sigma F$.
[c] Root mean square.

From the FVIIa-Y_T·sTF complex structure, it was evident that the trypsin 170 loop interacts with the active site region. This was illustrated by hydrogen bonding from the hydroxyl group of Tyr^{172} to the backbone nitrogen of Gln^{217} (3.1 Å) and the backbone carbonyl of Phe^{225} (2.5 Å) (Fig. 4, *A* and *B*). In addition, Tyr^{172} may further stabilize the 215–217 segment by favorable electrostatic aromatic interaction with Trp^{215} (closest ring carbons, 3.7–3.9 Å). In addition, the Tyr^{172} side chain displaces a water molecule (HOH_1) present in the FVIIa-WT structure, which may play a stabilizing role in the FVIIa-WT·sTF complex (Fig. 4*B*), supporting the increased amidolytic activity observed for the FVIIa-Y_T·sTF complex. It was also observed that a smaller serine at position 171, compared with glutamine in FVIIa-WT, seemed to enable the shorter 170 loop from trypsin to interact with the AL3 backbone (Fig. 5*A*).

The removal of the benzene and shortening of the hydroxyl group placement in FVIIa-S_T resulted in a loss of electron density for residues Ser^{172} and Pro^{173} in the 170 loop (Fig. 4*C*). This may result from competition of the shortened and possibly more mobile loop with a cacodylate ion found in both the FVIIa-S_T and FVIIa-WT structures (Fig. 4*C*). The structural data obtained for FVIIa-F_T revealed 170 loop and AL2–3 conformations very similar to that observed for FVIIa-Y_T with Phe^{172} occupying the same position as Tyr^{172}. The N terminus for the three variants was inserted in the activation pocket as in the FVIIa-WT·sTF crystal structure, possibly due to the presence of sTF and active site inhibitor. In general, shortening of the 170 loop seemed to affect the structural integrity of the TF-binding helix (residues 165–169) where the final turn of the helix was skewed for all three variants (Fig. 5*B*) with FVIIa-Y_T and -F_T ϕ/ψ angles of Asp^{167} and Cys^{168} outside the typical α-helix regions (Fig. 5*C*). This correlated with the observed loss of sTF affinity and lower extent of N terminus insertion for these variants, whereas FVIIa-S_T with ϕ/ψ angles closer to those of FVIIa-WT exhibited improved sTF affinity and a higher extent of N terminus insertion in the TF-bound complex. From these data, it seems that the orientation of the 170 loop and thus the structural integrity of TF-binding helix alter the extent to which the N terminus (Ile^{16}) can be inserted into the activation pocket as a consequence of sTF binding.

Molecular Dynamics Simulations Track Trp^{215} Movement—To allow for an unbiased observation of the dynamic behavior and a detailed understanding of the effects of Tyr^{172} on the protease domain, we performed 100 ns classical MD simulations for FVIIa-WT and the three variants without active site inhibitor and sTF. In addition, we also performed 100-ns classical MD simulations for FVIIa-WT in complex with sTF without active site inhibitor.

Our simulations show that AL1–3, including segment 215–217 that harbors Trp^{215} (supplemental Movies S1–S5), are highly flexible and undergo significant structural changes. The rearrangements are most pronounced in FVIIa-WT where Trp^{215} not only releases from the aryl binding pocket (S3-S4) but the S1 pocket collapses entirely as indicated by the short distance between Trp^{215} and Ser^{195} (Fig. 6, *A*–*C*). This suggests that the FVIIa molecule undergoes a transition where the 215–217 segment moves from an open conformation through an intermediate to a fully collapsed state where especially Trp^{215} occludes the substrate-binding region (Fig. 6, *A*–*D*). In the absence of sTF, this conformational transition from an open to a collapsed population is absent in FVIIa-Y_T but is reintroduced in the FVIIa-S_T and -F_T variants (Fig. 6*D*). Intriguingly, the

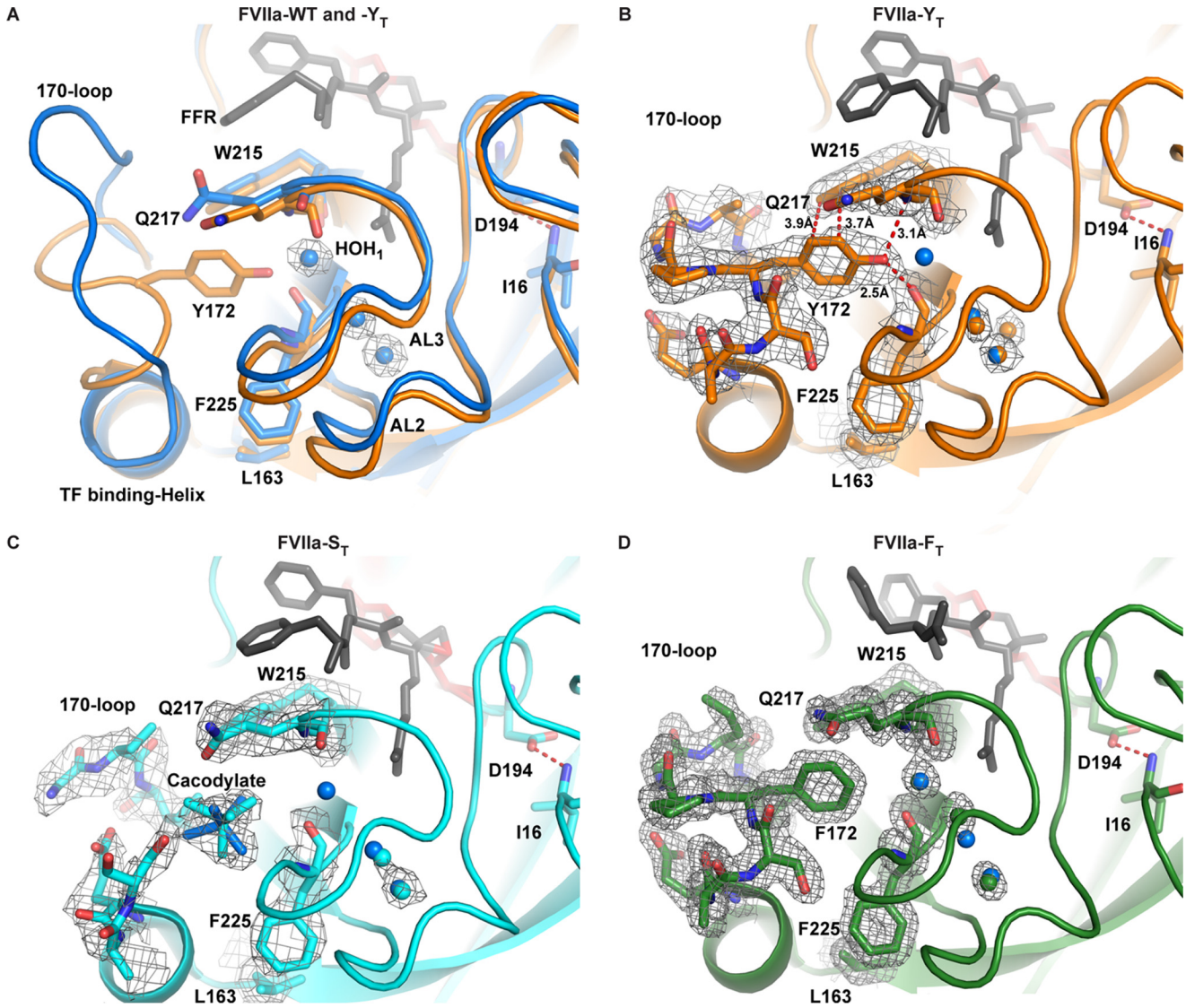

FIGURE 4. **Structural analysis reveals important role of Tyr^{172}.** *A*, comparison of FVIIa-WT (Protein Data Bank code 1dan; *dark blue*) and FVIIa-Y_T (*orange*) showing the insertion of Tyr^{172}, which displaces HOH_1. Water molecules found in the region of AL2–3 in FVIIa-WT are shown as *blue spheres* with all density contoured at the 1.0 σ level. Shown are the crystal structures of FVIIa-Y_T (*orange*) (*B*), FVIIa-S_T (*cyan*) (*C*), and FVIIa-F_T (*green*) (*D*) in complex with sTF and an active site inhibitor (FFR). Water molecules in the variants around the AL2–3 region are shown as *spheres* in their respective colors and for FVIIa-WT in *blue*. Hydrogen bonding from the OH group of Tyr^{172} to Gln^{217}/Phe^{225} is shown with *red dashed lines* together with possible stacking interaction with Trp^{215}. The N terminus was found to be in place in all variants, illustrated by the *red dotted line* from Asp^{194} to Ile^{16}. The cacodylate ion present in the FVIIa-WT structure is found in FVIIa-S_T but not in FVIIa-Y_T and -F_T as the pocket is occupied by Tyr/Phe.

215–217 segment is stabilized in the FVIIa-WT·sTF complex in a manner similar to that observed for FVIIa-Y_T (Fig. 6*D*). Additionally, it was observed that FVIIa-F_T displayed a significant collapse of the TF-binding helix in good agreement with the relatively low sTF affinity and that Trp^{215} is released from the S3 pocket into a position where it can interfere with substrate binding to S2/S3 sites and conceivably cause the low amidolytic activity. Furthermore, it seems that this mechanism is independent of N terminus insertion as the salt bridge between the amino group of Ile^{16} and Asp^{194} was present for the duration of all simulations.

Fluorescence Quenching Shows Changes to Tryptophan Accessibility—To correlate the MD simulations with an experimentally measurable quantity, we calculated SASA values for all tryptophans in the FVIIa protease domain throughout the simulation time course (Fig. 7, *A*–*C*). The SASA values were compared with results from a fluorescence quenching assay reporting on tryptophan solvent exposure by monitoring the loss of overall tryptophan fluorescence intensity upon addition of acrylamide (Fig. 7*D*) (34). According to the SASA calculations, three of the eight tryptophan residues (Trp^{61}, Trp^{207}, and Trp^{215}) were partially or fully exposed (Fig. 7*B*). This agreed well with the fluorescence quenching data where a significant level of quenching, or exposed tryptophans, was observed in FVIIa-WT (Fig. 7*D* and Table 3). The observed linearity of the quenching data allowed for the assumption of a collision quenching mechanism to predict the K_{sv} (43). In accordance with a collision quenching mechanism, increased quenching was observed with increasing temperatures (data not shown) (34).

Consistent with the distance plots (Fig. 6*D*), Trp^{215} exhibited varying SASA values over the time course of the simulations for

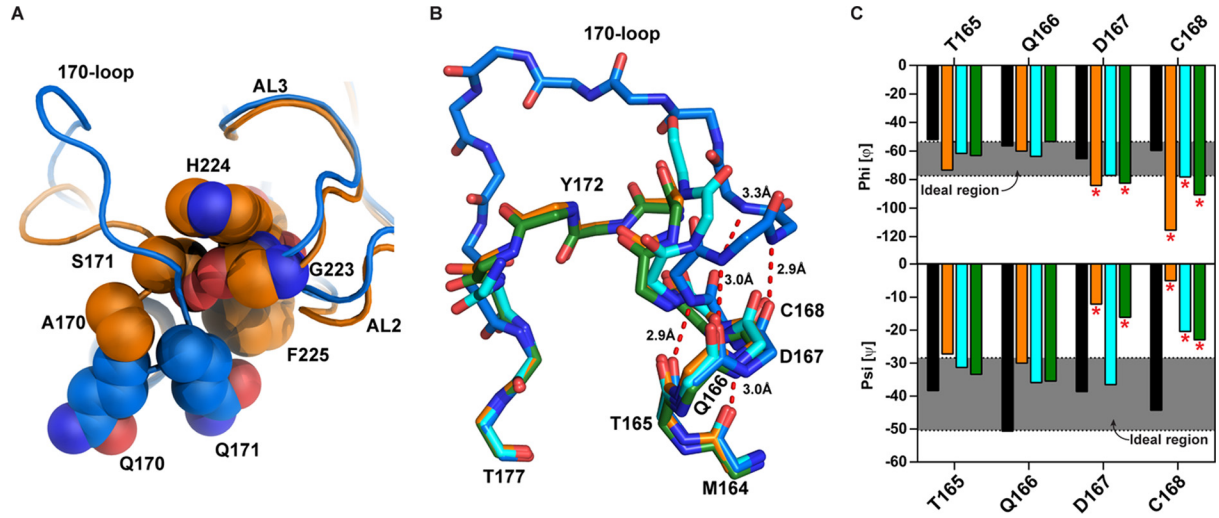

FIGURE 5. **Structural effects of 170 loop substitution.** *A*, alignment of the 170 loop from FVIIa-WT and FVIIa-Y_T showing removal of the possible Gln^{171} clash in FVIIa-Y_T by replacement to a serine at position 171. *B*, alignment of the 170 loop main chain of FVIIa-WT, -Y_T, -S_T, and-F_T showing changes to the main chain hydrogen bonding network of the TF-binding α-helices in the variants. *Red dashed lines* depict the backbone hydrogen bonding network of the FVIIa-WT α-helix. *C*, calculated ϕ/ψ angles for amino acids Thr^{165}–Cys^{168} in the beginning of the TF-binding helix with *gray* shaded areas being ideal ϕ/ψ angles as published by the European Molecular Biology Laboratory and * marking angles outside the ideal region.

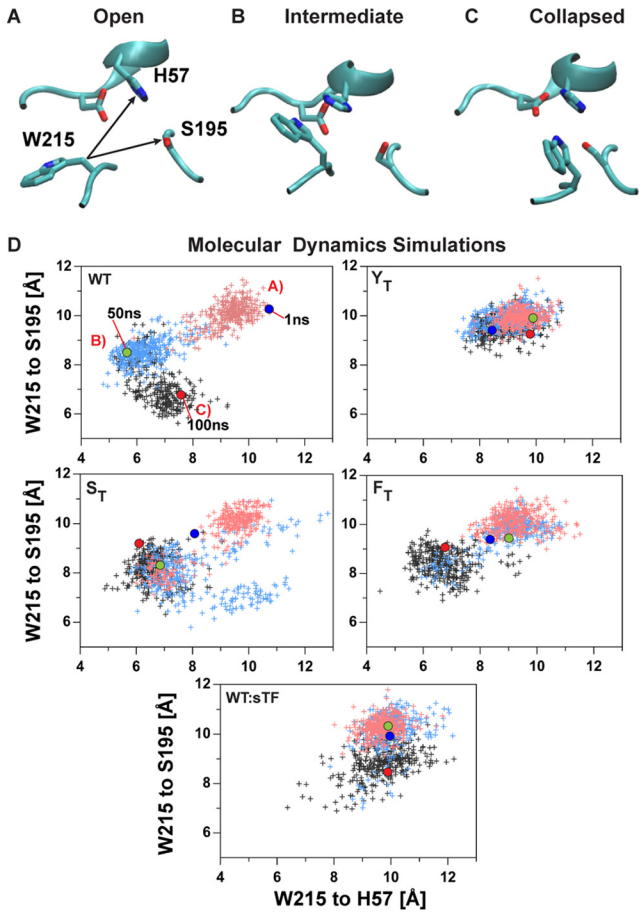

FIGURE 6. **Trp^{215} location in relation to the active site.** Representative conformations of segment 215–217 measured as Trp^{215} relative distances to the catalytic triad are shown. *A*, open; *B*, intermediate; *C*, collapsed. Each state is depicted on the scatter plots with their respective *letter*. *D*, scatter plots of Trp^{215} distance to the active residues His^{57} and Ser^{195}. Data from 0 to 33 ns are in *light red*, from 33 to 67 ns are in *light blue*, and from 67 to 100 ns are in *black*. Single data points from 1 ns are shown as a *blue filled dot*, from 50 ns are shown in *green*, and from 100 ns are shown in *red*. The calculated trajectories are available as supplemental data (supplemental Movies S1–S5).

FVIIa-WT, -S_T, and -F_T, whereas those of FVIIa-Y_T and FVIIa-WT·sTF showed lower and more stable levels (Fig. 7*C* and Table 3). In agreement with these observations, FVIIa-Y_T showed a significant decrease in quenching at 15 °C, whereas FVIIa-F_T was only moderately protected, and FVIIa-S_T showed a total quenching increase compared with FVIIa-WT (Fig. 7*D* and Table 3). The SASA values for Trp^{215} correlated well (Pearson r value of 0.99 and $p < 0.01$) with the K_{sv} values for the examined variants compared with Trp^{61}/Trp^{207} where the relationship between the measured and experimental data was less pronounced (Fig. 7, *E*–*G*). A control experiment with FFR added to all variants gave the expected normalization of quenching values to that of inhibited FVIIa-WT. This was in good agreement with the calculated SASA values, reflecting complete shielding of Trp^{215}, which should result in a significant decrease in overall quenching due to the large contribution from this residue to the total tryptophan surface-accessible area (~33%). These findings support that the acrylamide quenching is highly sensitive to the conformation of Trp^{215} even with the background signal from the remaining tryptophan residues.

Discussion

The TF-mediated allosteric regulation of FVIIa activity has been investigated for several decades, generating a wealth of experimental evidence for two distinct allosteric pathways (Fig. 1*B*). In the current model, the two pathways have a suggested common origin at the FVIIa-TF interface where especially the insertion of Met^{164} from FVIIa into a pocket of TF has proven essential for the propagation of the allosteric signal to the FVIIa active site (10, 23). From Met^{164}, the two pathways branch out with pathway I moving through the TF-binding helix to tether it and the 170 loop to the protease domain through Arg^{173} and Gly^{223} (24). Pathway II propagates through Leu^{163} and Phe^{225} to stabilize AL3, which in turn influences Ser^{185} in AL2, allowing N terminus insertion, which stabilizes a Val^{17} to Ala^{221a} interaction and the Cys^{191}-Cys^{220} disulfide pair (44). Here we attempt to elaborate on these two pathways and propose a more

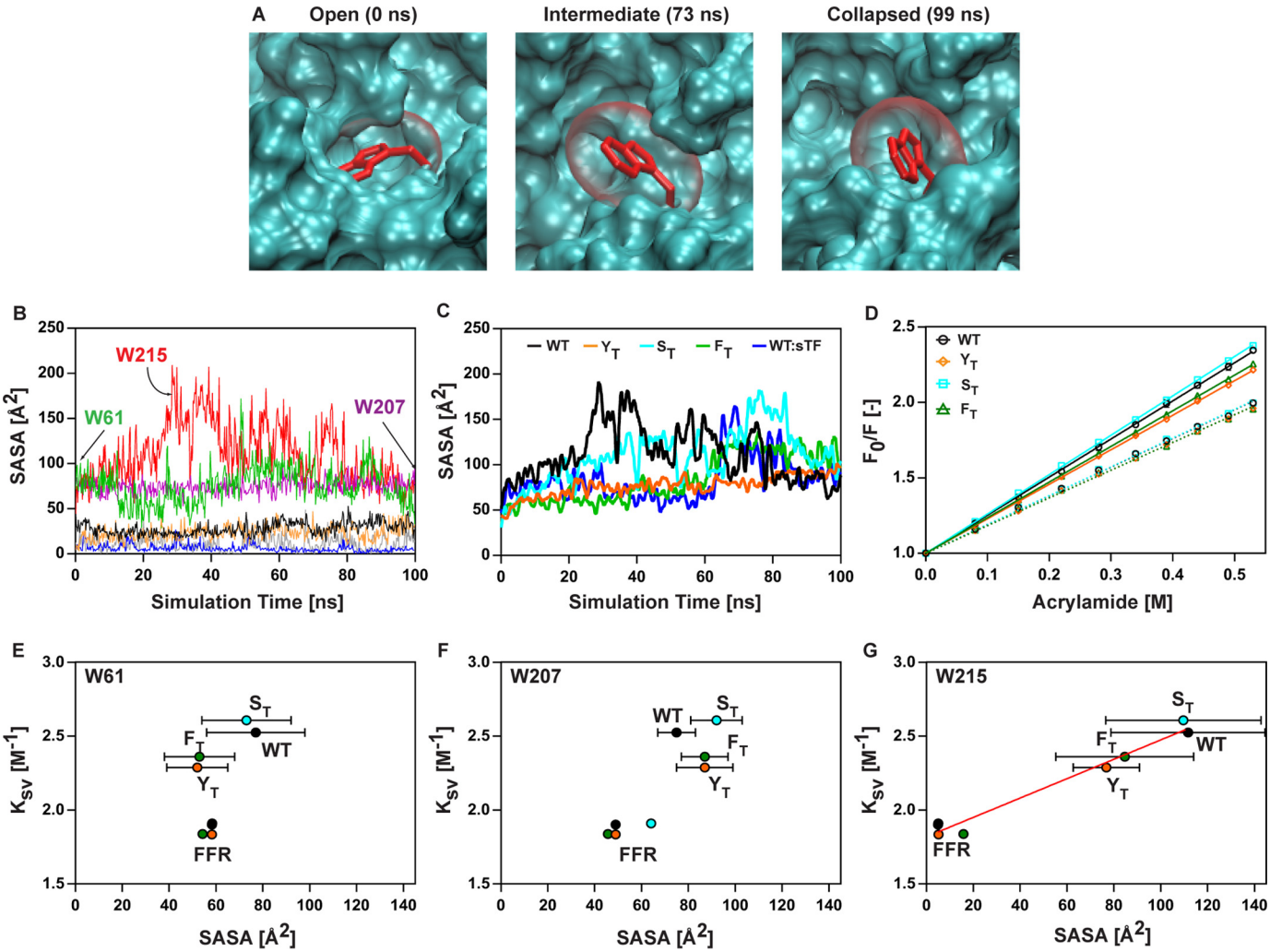

FIGURE 7. **Evaluation of tryptophan surface accessibility.** *A*, conformations of Trp^{215} in FVIIa-WT during MD simulations with van der Waals surface area in *red* in an open (0 ns), intermediate (73 ns), and collapsed conformations with collapsed S1 pocket (99 ns). *B*, plot of the calculated SASA values for all tryptophans of the protease domain during the simulation of FVIIa-WT. Trp^{29} (*black*), Trp^{51} (*orange*), Trp^{61} (*green*), Trp^{141} (*blue*), Trp^{207} (*purple*), Trp^{215} (*red*), and Trp^{237} (*gray*) are shown. *C*, calculated SASA values of Trp^{215} for all FVIIa variants during 100-ns MD simulations smoothened using a Savistsky and Golay algorithm. FVIIa-WT (*black*), FVIIa-WT·sTF (*blue*), FVIIa-Y_T (*orange*), FVIIa-S_T (*cyan*), and FVIIa-F_T (*green*) are shown. *D*, Stern-Volmer plot for the FVIIa variants as a function of acrylamide concentration. Shown are FVIIa-WT (○; *black*), FVIIa-Y_T (◇; *orange*), FVIIa-S_T (□; *cyan*) and FVIIa-F_T (△; *green*) in the presence (*dotted line*) or absence (*full line*) of FFR. Data are shown as mean ± S.D. (*error bars*) ($n = 2–4$) at 15 °C. *E–G*, scatter plots and correlation between the estimated K_{sv} constants and trajectory-averaged SASA values for Trp^{61}, Trp^{207}, and Trp^{215} for each individual FVIIa variant. SASA values with FFR present were calculated from the obtained crystal structures. The *error bars* indicating the standard deviation are shown for both *abscissa* and *ordinate*. A linear regression has been overlaid for Trp^{215} to illustrate correlation, which was statistically evaluated using a Pearson test.

TABLE 3

Tryptophan surface accessibility

SASA calculated from MD simulations and acrylamide K_{sv} values are shown as means with calculated S.E. in parentheses ($n = 2–4$).

	K_{sv}		
	−FFR	+FFR	Trp^{215} SASA
	M^{-1}		$Å^2$
FVIIa-WT	2.5 (0.008)	1.9 (0.01)	112 (33)
FVIIa-Y_T	2.3 (0.006)	1.8 (0.006)	77 (14)
FVIIa-S_T	2.6 (0.006)	1.9 (0.009)	110 (33)
FVIIa-F_T	2.4 (0.004)	1.8 (0.01)	85 (29)

complete molecular basis of TF-mediated allosteric enhancement of FVIIa activity.

The crystal structure of FVIIa-Y_T in complex with sTF revealed that Tyr^{172}, as in trypsin (45), is inserted into a cavity in the FVIIa protease domain, forming key hydrogen bonds with Gln^{217} and Phe^{225} and favorable electrostatic interaction with Trp^{215}. These key interactions, missing in the FVIIa-S_T and -F_T crystal structures, result in stabilization of segment 215–217 and AL3 in FVIIa-Y_T. Both Gln^{217} and Phe^{225} have been shown to be components of the two consensus TF-mediated allosteric pathways in FVIIa (5, 10, 46) that were recently suggested to encompass Trp^{215} (20). In addition, the hydroxyl group of Tyr^{172} displaces a water molecule (HOH_1; Fig. 4, *A* and *B*) found in the FVIIa-WT·sTF complex, which may result in a more stable hydrogen bond network, leading to the observed higher activity for the FVIIa-Y_T·sTF complex. It is quite likely that the introduced 170 loop from trypsin stabilizes allosteric pathway I via Tyr^{172} interactions in the absence of sTF, resulting in the increased amidolytic activity without complete N terminus insertion. In the presence of sTF, the inability of the FVIIa-Y_T protease domain N terminus to completely insert in the activation pocket may stem from the strain imposed by Tyr^{172} on the

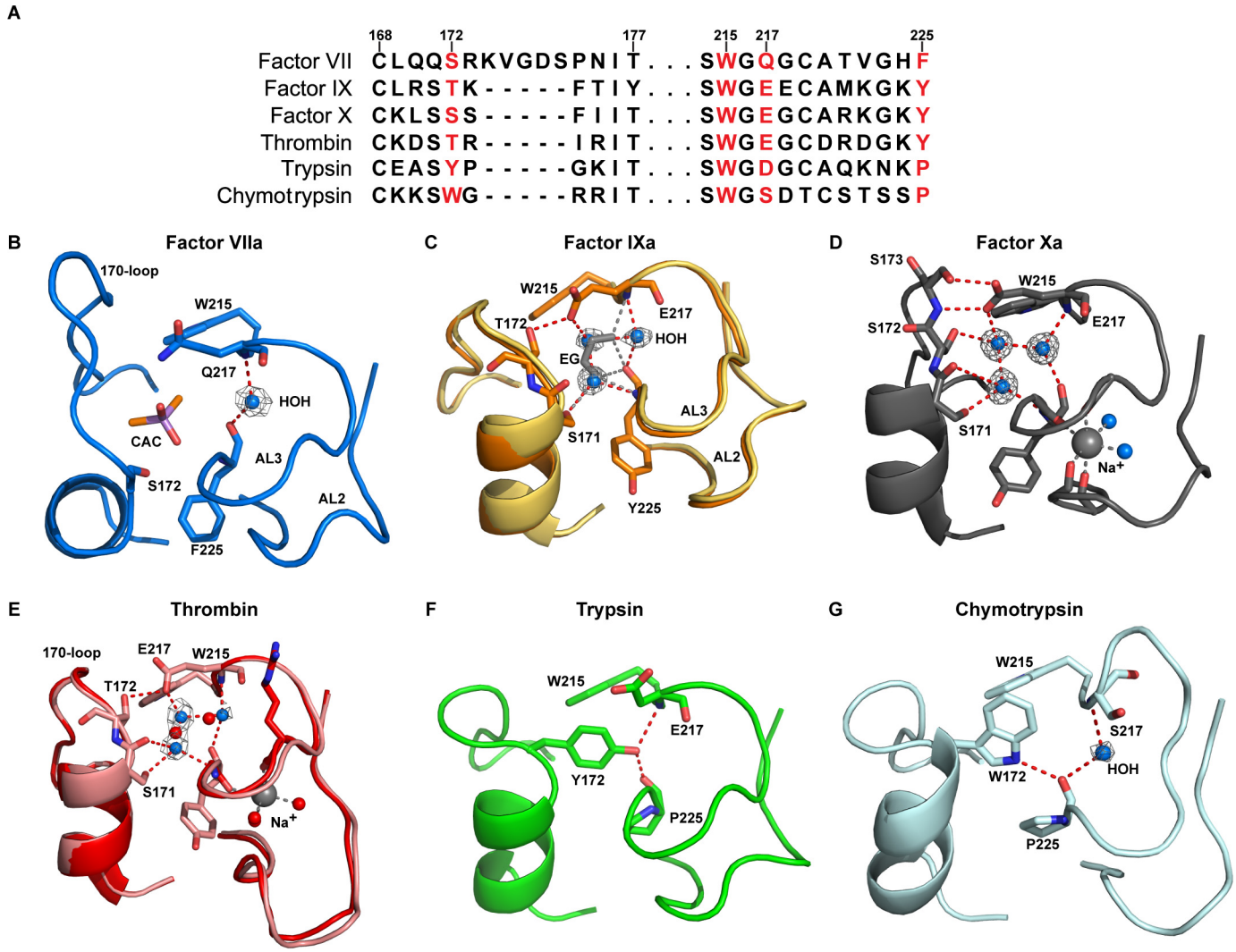

FIGURE 8. **Overview of 170 loop-mediated active site stabilization in trypsin-like serine proteases.** *A*, alignment of the selected proteases with residues corresponding to Tyr^{172}, Trp^{215}, Asp^{217}, and Pro^{225} in trypsin shown in *red*. Structural overviews of plausible 170 loop stabilization of the 215–217 segment in factor VIIa·sTF (*B*; Protein Data Bank code 1dan) with cacodylate (*CAC*), factor IXa (*C*; Protein Data Bank code 2wph in *dark orange* and Protein Data Bank code 2wpk in *light orange* with ethylene glycol (*EG*) in *gray*), factor Xa (*D*; Protein Data Bank code 2jkh) with Na^+ in *gray*, thrombin (*E*; Protein Data Bank code 1sgi in *light red* and Protein Data Bank code 1sg8 in *dark red*) with Na^+ in *gray* and coordinated waters in *red*, trypsin (*F*; Protein Data Bank code 1trn), and mouse chymotrypsin (*G*; Protein Data Bank code 2gch) are shown. Water molecules for all structures are shown as *blue spheres* with electron density contoured at $\sigma = 0.7$ with water hydrogen bonds (2.5–3.5 Å) as *red dotted lines* and ethylene glycol in *gray*.

170 loop by making direct contacts with AL2 and AL3. Although these interactions stabilize the 215–217 segment and AL3, leading to improved activity, they may interfere with allosteric pathway II and have a deleterious effect on the neighboring AL1. AL1 and AL2 along with other key interactions accommodate the N terminus. Previous studies have shown the critical role of Tyr^{172} in engineering substrate specificity (47) and Na^+ mimicry (48) in trypsin, warranting future studies probing the influence of Tyr^{172} on the conformation of segment 215–217 and the intrinsic activity of trypsin.

It has previously been reported that a five-residue truncation of the FVIIa 170 loop to the length found in trypsin resulted in a 3-fold decrease in amidolytic activity (12). The FVIIa-S_T variant investigated here has an identical 170 loop length but showed a 4-fold increase in amidolytic activity. From the crystal structures of FVIIa-S_T and -Y_T (Fig. 5*A*), it was evident that the additional changes relative to FVIIa-WT, specifically Gln^{171} to serine, removed a clash with AL2–3, allowing for the increased activity. This in turn suggests that shortening of the 170 loop in FVIIa-WT should result in gained activity if Gln^{171} was concomitantly mutated to a non-clashing residue (*e.g.* Ser or Ala). A similar effect was not observed for FVIIa-F_T as the activity was decreased significantly compared with that of FVIIa-WT. It is possible that Phe^{172} may help stabilize the S1 pocket by locating itself into the cavity normally found in FVIIa but is unable to stabilize the 215–217 segment, resulting in the observed decrease in amidolytic activity in combination with an increase in S1 pocket maturity. This effect became even more pronounced in the presence of sTF with the cofactor still able to mature the S1 pocket to FVIIa-WT levels through the proposed pathway II (10) but unable to potentiate amidolytic activity. The unfavorable conformation of the TF-binding helix may explain this as it is likely to result in the low extent of N terminus insertion, which without the effects of Tyr^{172} results in a signif-

icant destabilization of the whole activation pocket and the active site (5). In conclusion, despite incomplete N terminus insertion, a combination of several factors appears to contribute to the activity gain of FVIIa-Y_T, including 170 loop shortening, removal of a Gln^{171} clash, direct stabilization of 215–217 segment and AL3 through Tyr^{172}, and the displacement of a water molecule, which may enhance an allosteric pathway from Leu^{163} to the 215–217 segment.

The MD simulations allowed tracking of segment 215–217 movement in the three FVIIa 170 loop variants and FVIIa-WT. A clear picture emerged of FVIIa-Y_T being able to retain the open active conformation, whereas FVIIa-S_T, FVIIa-F_T, and FVIIa-WT collapsed into inactive closed states with Trp^{215} occluding the active site. Addition of sTF to FVIIa-WT stabilized segment 215–217 in the active open conformation, very similar to that of FVIIa-Y_T. This is in agreement with recent hydrogen-deuterium exchange mass spectrometry (20) where an increase in Trp^{215} backbone amide protection was seen upon sTF addition. The combined approach of SASA calculation and in-solution quenching used here allowed an elaboration on these observations. The approach showed a lower degree of quenching for the more active variants correlating with the SASA calculations, supporting the suggested activity-regulating mechanism observed in the MD simulations for the 170 loop swap variants. From these observations, we speculate that the final mechanism in the conversion of FVIIa into its catalytically competent state involves segment 215–217 moving from a collapsed to a more open conformation upon TF binding, allowing substrate access to the active site. The two allosteric pathways in FVIIa (10) may work in unison to allow for the stabilization of segment 215–217 in an open conformation because both stabilization of the 170 loop and AL1–3 through insertion of the N terminus are needed to maintain FVIIa in a fully catalytically competent state. The exact distribution of the suggested open and collapsed states in FVIIa, their relation to the N terminus insertion event, and whether this distribution is affected by binding of TF remain to be explored.

The ability of the trypsin 170 loop to stabilize the 215–217 segment in FVIIa prompted an investigation of the conformation surrounding the 170 loop and the active site in other trypsin-like proteases (Fig. 8). An interesting pattern emerges from the analyzed crystal structures with FVIIa and trypsin located at opposite ends of the spectrum with regard to reported activity. Three of the proteases involved in blood coagulation, factor IXa (49), factor Xa (50), and thrombin (51), all show possible stabilization of segment 215–217 via a conserved water hydrogen bond network between the Glu^{217} carboxyl group and the 170 loop. This mode of stabilization, however, may be more transient than the Tyr^{172}-mediated mechanism observed in trypsin. Ethylene glycol improves factor IXa activity ~20-fold (52) and may mimic the role of Tyr^{172}. In factor Xa, the presence of three consecutive serines (171–173) may mitigate the mobility of the water network (48), leading to higher intrinsic activity of this protease (53). In thrombin, recent work has shown that the apo form of thrombin is highly flexible (17) and exists in an open/collapsed equilibrium controlled by the position of the 215–217 segment (16, 18, 54) where the addition of Na^+ shifts the equilibrium in favor of the open form. We speculate that in the apo form the water network in thrombin facilitates a 170 loop-mediated stabilization of segment 215–217. In chymotrypsin, Trp^{172} makes a weak electrostatic interaction with the backbone of Pro^{225} and may stabilize the 215–217 segment by an edge-face stacking interaction with Trp^{215} (55). From the structures reviewed here, we speculate that stabilization of the 215–217 segment in an open conformation through 170 loop interactions could be a recurring theme in trypsin-like proteases (56) and that the structural mechanism behind this has diverged through evolution. This may accommodate the development of allosteric regulatory control as decreased intrinsic activity creates the need for cofactors to achieve full activity. Such intricate mechanisms in conjunction with the generation of new exosites due to cofactor binding allow for the necessary control of protease activity in the complex enzymatic cascades of blood coagulation.

Author Contributions—A. B. S. designed the research, conducted experiments, analyzed the results, and wrote and revised the manuscript. J. J. M. designed the research, conducted the molecular dynamics simulations, and wrote the manuscript. L. A. S. and A. A. P. supported the experiments and analyzed results. H. Ø., M. T. O., and O. H. O. designed the research, reviewed the results, and revised the manuscript. P. S. G. designed the research, reviewed the results, and wrote and revised the manuscript.

Acknowledgments—We thank Michael P. Petersen and Anette S. Petersen for excellent technical assistance. We also thank Hanne Grøn, Grant E. Blouse, and Egon Persson for valuable scientific discussions and comments.

References

1. Davie, E. W., Fujikawa, K., and Kisiel, W. (1991) The coagulation cascade: initiation, maintenance, and regulation. *Biochemistry* **30,** 10363–10370
2. Banner, D. W., D'Arcy, A., Chène, C., Winkler, F. K., Guha, A., Konigsberg, W. H., Nemerson, Y., and Kirchhofer, D. (1996) The crystal structure of the complex of blood coagulation factor VIIa with soluble tissue factor. *Nature* **380,** 41–46
3. Huber, R., and Bode, W. (1978) Structural basis of the activation and action of trypsin. *Acc. Chem. Res.* **266,** 114–122
4. Higashi, S., Nishimura, H., Aita, K., and Iwanaga, S. (1994) Identification of regions of bovine factor VII essential for binding to tissue factor. *J. Biol. Chem.* **269,** 18891–18898
5. Rand, K. D., Andersen, M. D., Olsen, O. H., Jørgensen, T. J., Ostergaard, H., Jensen, O. N., Stennicke, H. R., and Persson, E. (2008) The origins of enhanced activity in factor VIIa analogs and the interplay between key allosteric sites revealed by hydrogen exchange mass spectrometry. *J. Biol. Chem.* **283,** 13378–13387
6. Pike, A. C., Brzozowski, A. M., Roberts, S. M., Olsen, O. H., and Persson, E. (1999) Structure of human factor VIIa and its implications for the triggering of blood coagulation. *Proc. Natl. Acad. Sci. U.S.A.* **96,** 8925–8930
7. Persson, E., Kjalke, M., and Olsen, O. H. (2001) Rational design of coagulation factor VIIa variants with substantially increased intrinsic activity. *Proc. Natl. Acad. Sci. U.S.A.* **98,** 13583–13588
8. Ohkubo, Y. Z., Morrissey, J. H., and Tajkhorshid, E. (2010) Dynamical view of membrane binding and complex formation of human factor VIIa and tissue factor. *J. Thromb. Haemost.* **8,** 1044–1053
9. McCallum, C. D., Hapak, R. C., Neuenschwander, P. F., Morrissey, J. H., and Johnson, A. E. (1996) The location of the active site of blood coagulation factor VIIa above the membrane surface and its reorientation upon association with tissue factor: a fluorescence energy transfer study. *J. Biol. Chem.* **271,** 28168–28175
10. Persson, E., and Olsen, O. H. (2011) Allosteric activation of coagulation

factor VIIa. *Front. Biosci.* **16,** 3156–3163
11. Persson, E., Bak, H., Østergaard, A., and Olsen, O. H. (2004) Augmented intrinsic activity of Factor VIIa by replacement of residues 305, 314, 337 and 374: evidence of two unique mutational mechanisms of activity enhancement. *Biochem. J.* **379,** 497–503
12. Soejima, K., Mizuguchi, J., Yuguchi, M., Nakagaki, T., Higashi, S., and Iwanaga, S. (2001) Factor VIIa modified in the 170 loop shows enhanced catalytic activity but does not change the zymogen-like property. *J. Biol. Chem.* **276,** 17229–17235
13. Gandhi, P. S., Chen, Z., Mathews, F. S., and Di Cera, E. (2008) Structural identification of the pathway of long-range communication in an allosteric enzyme. *Proc. Natl. Acad. Sci. U.S.A.* **105,** 1832–1837
14. Pozzi, N., Vogt, A. D., Gohara, D. W., and Di Cera, E. (2012) Conformational selection in trypsin-like proteases. *Curr. Opin. Struct. Biol.* **22,** 421–431
15. Bah, A., Garvey, L. C., Ge, J., and Di Cera, E. (2006) Rapid kinetics of Na^+ binding to thrombin. *J. Biol. Chem.* **281,** 40049–40056
16. Niu, W., Chen, Z., Gandhi, P. S., Vogt, A. D., Pozzi, N., Pelc, L. A., Zapata, F., and Di Cera, E. (2011) Crystallographic and kinetic evidence of allostery in a trypsin-like protease. *Biochemistry* **50,** 6301–6307
17. Lechtenberg, B. C., Johnson, D. J., Freund, S. M., and Huntington, J. A. (2010) NMR resonance assignments of thrombin reveal the conformational and dynamic effects of ligation. *Proc. Natl. Acad. Sci. U.S.A.* **107,** 14087–14092
18. Vogt, A. D., Chakraborty, P., and Di Cera, E. (2015) Kinetic dissection of the pre-existing conformational equilibrium in the trypsin fold. *J. Biol. Chem.* **290,** 22435–22445
19. Huntington, J. A., and Esmon, C. T. (2003) The molecular basis of thrombin allostery revealed by a 1.8 Å structure of the "slow" form. *Structure* **11,** 469–479
20. Song, H., Olsen, O. H., Persson, E., and Rand, K. D. (2014) Sites involved in intra- and interdomain allostery associated with the activation of factor VIIa pinpointed by hydrogen-deuterium exchange and electron transfer dissociation mass spectrometry. *J. Biol. Chem.* **289,** 35388–35396
21. Madsen, J. J., Persson, E., and Olsen, O. H. (2015) Tissue factor activates allosteric networks in factor VIIa through structural and dynamic changes. *J. Thromb. Haemost.* **13,** 262–267
22. Freskgård, P. O., Olsen, O. H., and Persson, E. (1996) Structural changes in factor VIIa induced by Ca^{2+} and tissue factor studied using circular dichroism spectroscopy. *Protein Sci.* **5,** 1531–1540
23. Persson, E., Nielsen, L. S., and Olsen, O. H. (2001) Substitution of aspartic acid for methionine-306 in factor VIIa abolishes the allosteric linkage between the active site and the binding interface with tissue factor. *Biochemistry* **40,** 3251–3256
24. Persson, E., and Olsen, O. H. (2009) Activation loop 3 and the 170 loop interact in the active conformation of coagulation factor VIIa. *FEBS J.* **276,** 3099–3109
25. Ursby, T., Unge, J., Appio, R., Logan, D. T., Fredslund, F., Svensson, C., Larsson, K., Labrador, A., and Thunnissen, M. M. (2013) The macromolecular crystallography beamline I911-3 at the MAX IV laboratory. *J. Synchrotron Radiat.* **20,** 648–653
26. Kabsch, W. (2010) XDS. *Acta Crystallogr. D Biol. Crystallogr.* **66,** 125–132
27. McCoy, A. J., Grosse-Kunstleve, R. W., Adams, P. D., Winn, M. D., Storoni, L. C., and Read, R. J. (2007) Phaser crystallographic software. *J. Appl. Crystallogr.* **40,** 658–674
28. Afonine, P. V., Grosse-Kunstleve, R. W., Echols, N., Headd, J. J., Moriarty, N. W., Mustyakimov, M., Terwilliger, T. C., Urzhumtsev, A., Zwart, P. H., and Adams, P. D. (2012) Towards automated crystallographic structure refinement with phenix.refine. *Acta Crystallogr. D Biol. Crystallogr.* **68,** 352–367
29. Adams, P. D., Afonine, P. V., Bunkóczi, G., Chen, V. B., Davis, I. W., Echols, N., Headd, J. J., Hung, L.-W., Kapral, G. J., Grosse-Kunstleve, R. W., McCoy, A. J., Moriarty, N. W., Oeffner, R., Read, R. J., Richardson, D. C., Richardson, J. S., Terwilliger, T. C., and Zwart, P. H. (2010) PHENIX: a comprehensive Python-based system for macromolecular structure solution. *Acta Crystallogr. D Biol. Crystallogr.* **66,** 213–221
30. Davis, I. W., Leaver-Fay, A., Chen, V. B., Block, J. N., Kapral, G. J., Wang, X., Murray, L. W., Arendall, W. B., 3rd, Snoeyink, J., Richardson, J. S., and Richardson, D. C. (2007) MolProbity: all-atom contacts and structure validation for proteins and nucleic acids. *Nucleic Acids Res.* **35,** W375–W383
31. Winn, M. D., Murshudov, G. N., and Papiz, M. Z. (2003) Macromolecular TLS refinement in REFMAC at moderate resolutions. *Methods Enzymol.* **374,** 300–321
32. Emsley, P., Lohkamp, B., Scott, W. G., and Cowtan, K. (2010) Features and development of Coot. *Acta Crystallogr. D Biol. Crystallogr.* **66,** 486–501
33. Lutz, H., and Luisi, P. L. (1983) Correction for inner filter effects in fluorescence spectroscopy. *Helv. Chim. Acta* **66,** 1929–1935
34. Lakowicz, J. (2007) *Principles of Fluorescence Spectroscopy*, 3rd Ed., pp. 277–293, Springer, New York
35. Sichler, K., Banner, D. W., D'Arcy, A., Hopfner, K. P., Huber, R., Bode, W., Kresse, G.-B., Kopetzki, E., and Brandstetter, H. (2002) Crystal structures of uninhibited factor VIIa link its cofactor and substrate-assisted activation to specific interactions. *J. Mol. Biol.* **322,** 591–603
36. Phillips, J. C., Braun, R., Wang, W., Gumbart, J., Tajkhorshid, E., Villa, E., Chipot, C., Skeel, R. D., Kalé, L., and Schulten, K. (2005) Scalable molecular dynamics with NAMD. *J. Comput. Chem.* **26,** 1781–1802
37. MacKerell, A. D., Bashford, D., Bellott, M., Dunbrack, R. L., Evanseck, J. D., Field, M. J., Fischer, S., Gao, J., Guo, H., Ha, S., Joseph-McCarthy, D.,Kuchnir, L., Kuczera, K., Lau, F. T., Mattos, C., Michnick, S., Ngo, T., Nguyen, D. T., Prodhom, B., Reiher, W. E., Roux, B., Schlenkrich, M., Smith, J. C., Stote, R., Straub, J., Watanabe, M., Wiórkiewicz-Kuczera, J., Yin, D., and Karplus, M. (1998) All-atom empirical potential for molecular modeling and dynamics studies of proteins. *J. Phys. Chem. B* **102,** 3586–3616
38. Jorgensen, W. L., Chandrasekhar, J., Madura, J. D., Impey, R. W., and Klein, M. L. (1983) Comparison of simple potential functions for simulating liquid water. *J. Chem. Phys.* **79,** 926
39. Martyna, G. J., Tobias, D. J., and Klein, M. L. (1994) Constant pressure molecular dynamics algorithms. *J. Chem. Phys.* **101,** 4177
40. Feller, S. E., Zhang, Y., Pastor, R. W., and Brooks, B. R. (1995) Constant pressure molecular dynamics simulation: the Langevin piston method. *J. Chem. Phys.* **103,** 4613
41. Essmann, U., Perera, L., Berkowitz, M. L., Darden, T., Lee, H., and Pedersen, L. G. (1995) A smooth particle mesh Ewald method. *J. Chem. Phys.* **103,** 8577–8593
42. Humphrey, W., Dalke, A., and Schulten, K. (1996) VMD: visual molecular dynamics. *J. Mol. Graph.* **14,** 33–38
43. Eftink, M. R., and Ghiron, C. A. (1981) Fluorescence quenching studies with proteins. *Anal. Biochem.* **114,** 199–227
44. Olsen, O. H., Rand, K. D., Østergaard, H., and Persson, E. (2007) A combined structural dynamics approach identifies a putative switch in factor VIIa employed by tissue factor to initiate blood coagulation. *Protein Sci.* **16,** 671–682
45. Gaboriaud, C., Serre, L., Guy-Crotte, O., Forest, E., and Fontecilla-Camps, J. C. (1996) Crystal structure of human trypsin 1: unexpected phosphorylation of Tyr151. *J. Mol. Biol.* **259,** 995–1010
46. Petrovan, R. J., and Ruf, W. (2000) Role of residue Phe225 in the cofactor-mediated, allosteric regulation of the serine protease coagulation factor VIIa. *Biochemistry* **39,** 14457–14463
47. Hedstrom, L., Perona, J. J., and Rutter, W. J. (1994) Converting trypsin to chymotrypsin: residue 172 is a substrate specificity determinant. *Biochemistry* **33,** 8757–8763
48. Page, M. J., Bleackley, M. R., Wong, S., MacGillivray, R. T., and Di Cera, E. (2006) Conversion of trypsin into a Na^+-activated enzyme. *Biochemistry* **45,** 2987–2993
49. Zögg, T., and Brandstetter, H. (2009) Structural basis of the cofactor- and substrate-assisted activation of human coagulation factor IXa. *Structure* **17,** 1669–1678
50. Salonen, L. M., Bucher, C., Banner, D. W., Haap, W., Mary, J. L., Benz, J., Kuster, O., Seiler, P., Schweizer, W. B., and Diederich, F. (2009) Cation-π interactions at the active site of factor Xa: dramatic enhancement upon stepwise N-alkylation of ammonium ions. *Angew. Chem. Int. Ed. Engl.* **48,** 811–814
51. Pineda, A. O., Carrell, C. J., Bush, L. A., Prasad, S., Caccia, S., Chen, Z.-W., Mathews, F. S., and Di Cera, E. (2004) Molecular dissection of Na^+ binding to thrombin. *J. Biol. Chem.* **279,** 31842–31853
52. Sturzebecher, J., Kopetzki, E., Bode, W., and Hopfner, K. P. (1997) Dra-

matic enhancement of the catalytic activity of coagulation factor IXa by alcohols. *FEBS Lett.* **412,** 295–300
53. Hopfner, K. P., Brandstetter, H., Karcher, A., Kopetzki, E., Huber, R., Engh, R. A., and Bode, W. (1997) Converting blood coagulation factor IXa into factor Xa: dramatic increase in amidolytic activity identifies important active site determinants. *EMBO J.* **16,** 6626–6635
54. Carter, W. J., Myles, T., Gibbs, C. S., Leung, L. L., and Huntington, J. A. (2004) Crystal structure of anticoagulant thrombin variant E217K provides insights into thrombin allostery. *J. Biol. Chem.* **279,** 26387–26394
55. Cohen, G. H., Silverton, E. W., and Davies, D. R. (1981) Refined crystal structure of gamma-chymotrypsin at 1.9 Å resolution. Comparison with other pancreatic serine proteases. *J. Mol. Biol.* **148,** 449–479
56. Gohara, D. W., and Di Cera, E. (2011) Allostery in trypsin-like proteases suggests new therapeutic strategies. *Trends Biotechnol.* **29,** 577–585